JOURNAL OF AIRCRAFT
Vol. 48, No. 2, March–April 2011

Dynamic Response to Turbulence of Tethered Lighter-Than-Air Platforms

S. Redi,* G. S. Aglietti,† A. R. Tatnall,‡ and T. Markvart§
University of Southampton, Southampton, England SO17 1BJ, United Kingdom

DOI: 10.2514/1.C031137

The study presented in this paper concerns the development of an algorithm, based on finite element analysis, for the dynamic simulation of a tethered lighter-than-air balloon when subjected to operational conditions. The main features of the algorithm are described, highlighting the advantages of this approach when performing dynamic analysis. The input parameters considered in the method are derived from experimental and simulated data, which are elaborated to obtain the static and dynamic atmospheric properties in terms of mean windspeed profile, discrete gusts, and continuous turbulence. In particular, the algorithm is employed to perform a thorough analysis of a specific high-altitude tethered platform operating in a realistic design scenario. The dynamic behavior of the system is evaluated in terms of displacements and tether forces. The results, even though they are obtained for a specific example application, demonstrate the general viability of the algorithm proposed for the evaluation of the dynamic response of high-altitude tethered platforms and for the preliminary assessment of the technical feasibility of these systems.

Nomenclature

A_{Comp}	=	composite cross section
B	=	buoyancy
c	=	Weibull scale parameter
$\text{Cdf}(V_{\text{Wind}})$	=	cumulative distribution function
C_D^B	=	balloon drag coefficient
C_D^{segm}	=	tether segment drag coefficient
C_L^{segm}	=	tether segment lift coefficient
d_{teth}	=	tether diameter
D_B	=	balloon aerodynamic drag
D_{segm}	=	tether segment aerodynamic drag
E_{Comp}	=	composite elastic modulus
F	=	force
f	=	frequency
F_0	=	force amplitude
g	=	gravity acceleration
H	=	gust gradient length
k	=	Weibull shape parameter
L_{segm}	=	tether segment aerodynamic lift
L_u, L_v, L_w	=	turbulence scale length
len_{segm}	=	tether segment length
$\text{len}^{\text{tether}}$	=	tether length
m	=	mass
m^*	=	mass ratio
m_e	=	total mass (including added mass)
m_{Fluid}	=	displaced fluid mass
m^*_{Crit}	=	critical mass
$\text{Pdf}(V_{\text{Wind}})$	=	probability density function
T	=	oscillation period
V_{Gust}	=	gust windspeed
V_{Max}	=	maximum gust windspeed
V_{Wind}	=	absolute windspeed
$\overline{V}_{\text{wind}}$	=	mean windspeed
V^R_{Wind}	=	relative windspeed
Vol_B	=	balloon volume
W_{Env}	=	envelope weight
W_{Gas}	=	lifting gas weight
$W_{\text{P/L}}$	=	payload weight
x	=	gust penetration distance
Y_{Amp}	=	oscillation amplitude
α	=	tether inclination angle
Γ	=	gamma function
ρ_{Air}	=	atmospheric density
ρ_{Gas}	=	lifting gas density
ς	=	damping ratio
σ_U	=	ultimate stress
σ_u,σ_v,σ_w	=	turbulence intensities
Φ	=	turbulence spectrum
ϕ_B	=	balloon diameter
σ^2_{Wind}	=	windspeed variance
Ω	=	wave number
ω_n	=	natural frequency

Received 11 June 2010; revision received 4 October 2010; accepted for publication 9 November 2010.

*Ph.D. Candidate, School of Engineering Sciences, Highfield.
†Reader, School of Engineering Sciences, Highfield. Member AIAA.
‡Senior Lecturer, School of Engineering Sciences, Highfield.
§Professor, School of Engineering Sciences, Highfield.

I. Introduction

TETHERED lighter-than-air balloons (also referred to as aerostats), in order to be cost effective, need to be capable of continuous operations for long periods of time in which different weather conditions, including strong winds and atmospheric turbulence, can occur. Modern applications of tethered aerostats range from scientific to military purposes [1,2] requiring a high degree of reliability during the entire operational phase. The fact that these systems are not usually equipped with a propulsion unit, and their weight is comparable to the one of the fluid they displace, implies that their dynamic behavior is determined by the characteristics of the surrounding atmosphere. The study of the dynamic response of the system when subjected to atmospheric turbulence is therefore crucial during the design phase of a tethered lighter-than-air platform, since it allows the determination of important parameters like the forces along the mooring tether and the displacements of the balloon, which have to comply with the project requirements.

Several studies have been conducted in the past, most of which deal with the development of mathematical models to define the dynamic behavior of tethered streamlined aerostats when subjected to operational atmospheric conditions [3,4]. More recent publications [5,6] present different dynamic simulations performed to assess the feasibility of very high altitude tethered balloon systems. In particular, the work conducted at the McGill University

has been focused on the design and analysis of the dynamics of systems based on lighter-than-air technology. The resulting publications [7–9] therefore contain a large wealth of information.

The study presented in this paper introduces an alternative approach for the evaluation of the response of a tethered spherical aerostat, performing a full three-dimensional (3-D) dynamic nonlinear simulation based on a finite element model (FEM). The proposed method has been developed and preliminarily validated by Aglietti [10] in the case of horizontal gusts. Here, the model is further extended and employed to perform a complete analysis of a lighter-than-air tethered platform operating in a realistic design scenario that takes into account gusts along the three directions, vortex-induced vibrations, and simulated continuous turbulence. The results, including displacements and forces along the tether, are used to prove the operational viability of this tool and to preliminarily assess the technical feasibility of the system under analysis.

The particular example application considered concerns the development of a lighter-than-air spherical platform that would be used to support an array of photovoltaic (PV) cells to produce power at a high altitude in order to overcome the problems related to the cloud coverage that, in many countries in northern Europe (like the United Kingdom), has always limited the extensive exploitation of the solar resource. The power generated would be transmitted to the ground via the mooring tether, which would also be capable of withstanding the loads produced by the aerodynamic forces on the system. The concept definition and possible technical and nontechnical issues involved in the project are presented in [11]. On the other hand, the present publication is focused on the dynamic analysis of this particular system through the employment of a method that could be easily adapted for the evaluation of the behavior of general tethered spherical balloons. Readers interested in knowing more about the particular concept employed in the analysis should refer to past publications (e.g., [11]). After an introduction of the main characteristics of the proposed approach (Sec. II), the evaluation of atmospheric conditions in terms of mean wind profile (experimental), discrete gusts, and turbulence (simulated) is presented (Sec. III). The method described is then applied to the particular case of the aerostat for electrical power generation (AEPG), in Sec. IV, in order to evaluate the response of the system and assess the technical feasibility of the tethered platform. Results are discussed and conclusions inferred in Sec. V.

II. Model Description

The FEM model used in this study has already been extensively described in [10]. In this section, the key points are recalled in order to identify the main characteristics of the model and introduce the possible advantages of this approach. The tethered balloon system, modeled using a commercial FE software (ANSYS), is discretized into a defined number of elements and nodes: the first node representing the center of mass of the spherical balloon, and the last one corresponding to the ground station. The number of nodes and segments is determined based on considerations about the convergence of the results. The balloon is modeled as a six-degree-of-freedom structural mass concentrated on a single node, while the tether segments are modeled as standard FEM beam elements with tension, compression, torsion, and bending capabilities, which can include the effect of large deflections. The choice of beam elements instead of rods allows the simulation to take into account the bending stiffness of the tether that, in some cases, might not be negligible. The material properties include density, elastic modulus, and Poisson's ratio. For what concerns the material damping, although this characteristic can be modeled in ANSYS, its effect is assumed small compared with other sources of damping (e.g., aerodynamic damping), and it is not included in the present model.

The forces due to the buoyancy, weight, and aerodynamic effects are assumed to be applied on the nodes connecting two consecutive elements. The constraint on the ground is modeled as a pin, releasing the rotation about the three axes. Figure 1 presents the discretization of the system and the reference frame used for calculations.

Focusing on node 1 (balloon), the loads to be considered are the buoyancy B (in newtons) generated by the displaced fluid and the aerodynamic drag D_B (in newtons) due to the interaction with the windspeed. The buoyancy has to overcome the weight of the lifting gas W_{Gas} (in newtons), the envelope W_{Env} (in newtons), and the payload $W_{\text{P/L}}$ (in newtons). Since the mass of the balloon is comparable with that of the displaced fluid, a dynamic simulation needs to include the contribution of the added mass. Therefore, this contribution has been taken into account and assumed as half the value of the displaced fluid mass [12], considering the spherical shape of the balloon. It should be pointed out that this assumption is valid for irrotational flows, and a more accurate estimate should be considered for applications in which the vorticity effects are significant [13]. Nevertheless, the practical validity of the theoretical results in [12] has been confirmed in previous publications [14], even in the case of separated flows.

Assuming the envelope is fully inflated at operational altitude, the buoyancy and weight of the lifting gas depends on the atmospheric pressure value at that height. The density of the atmosphere ρ_{Air} can be determined, starting from the temperature and pressure profiles provided by the standard atmospheric model [15] and treating air as a perfect gas. Assuming that the internal pressure and temperature are the same as the external atmospheric pressure and temperature (no superheating), and considering the lifting gas as a perfect gas, it is possible to determine the density of the gas at an operational altitude ρ_{Gas} (in kilograms per cubic meter). The standard atmospheric model and the perfect gas equations are included in the model, which updates the values of the gas densities as the vertical position of the balloon changes during the simulation.

Considering the balloon fully inflated at operational altitude, the buoyancy and weight of the lifting gas (in newtons) can be determined as

$$B = \text{Vol}_B \cdot \rho_{\text{Air}} \cdot g \tag{1}$$

$$W_{\text{Gas}} = \text{Vol}_B \cdot \rho_{\text{Gas}} \cdot g \tag{2}$$

where g is the acceleration of gravity (9.81 m/s^2), and the volume of the spherical balloon (in cubic meters) can be calculated from the diameter ϕ_B (in meters).

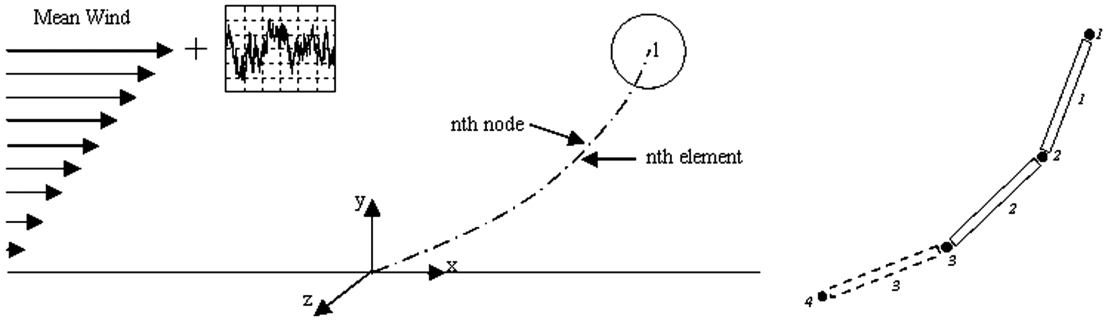

Fig. 1 FEM discretization and reference frame.

Furthermore the determination of the atmospheric conditions (see Sec. III) at operational altitude leads to the definition of the drag force on the balloon, calculated as

$$D_B = \frac{1}{2}\rho_{\text{Air}}(V^R_{\text{Wind}})^2 C^B_D \frac{\phi^2_B}{4}\pi \tag{3}$$

where V^R_{Wind} is the absolute value of the relative windspeed vector, defined as the difference between the velocity of the balloon and the windspeed, which varies with the altitude above the ground, as presented in Sec. III.A. The drag is a vector oriented in the same direction as the relative wind. As the simulation is 3-D, the force will have three components in the reference frame considered in the model. C^B_D is the drag coefficient of the balloon, which depends on the Reynolds number considered: i.e., on the velocity of the flow, the size of the balloon, and the characteristics of the fluid.

For what concerns the forces relative to the tether segments, the weight of each segment is determined by simply dividing the total weight of the tether by the number of segments set for the discretization. The aerodynamic forces (drag and lift) on the elements can be determined as a function of the relative windspeed V^R_{Wind}:

$$D_{\text{segm}} = \tfrac{1}{2}\rho_{\text{Air}}(V^R_{\text{Wind}})^2 C^{\text{segm}}_D \text{len}_{\text{segm}} d_{\text{teth}} \tag{4}$$

$$L_{\text{segm}} = \tfrac{1}{2}\rho_{\text{Air}}(V^R_{\text{Wind}})^2 C^{\text{segm}}_L \text{len}_{\text{segm}} d_{\text{teth}} \tag{5}$$

where d_{teth} and len_{segm} are the tether diameter and segment length, respectively. The drag and lift coefficient depend on the segment inclination angle α with respect to the relative windspeed, as in [12]:

$$C^{\text{segm}}_D = 0.02 + 1.1 \cdot \sin^3(\alpha) \tag{6}$$

$$C^{\text{segm}}_L = 1.1 \cdot \cos(\alpha) \cdot \sin^2(\alpha) \tag{7}$$

The determination of the tether segment orientation and the evaluation of the inclination angle α are described in more detail in [10]. As in the case of the drag force on the balloon, the aerodynamic forces on the segments are projected in the reference frame shown in Fig. 1.

The simulation operates with an iterative scheme, as the one presented in Fig. 2. The time domain (duration of the simulation) is divided in time steps and, at each time step, the simulation calculates the displacements of the structure and the forces in the elements. The solution of each time step is used to update the loads on the system, which depend on the position and velocity of each node. The updated loads are used as input for the following time-step calculations.

First, the mean windspeed profile is applied until equilibrium is reached. Starting from this steady-state condition, the atmospheric turbulence is superimposed and applied to the balloon to assess the dynamic response.

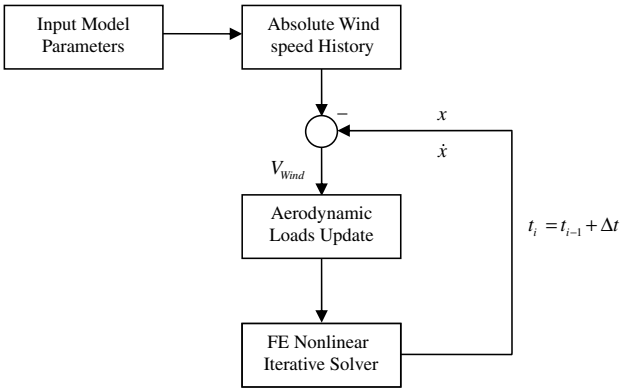

Fig. 2 FEM simulation iterative scheme.

III. Operational Conditions

The definition of the conditions in which the system is due to operate is essential to provide the input values to the simulation. In particular, it is important to define the mean windspeed profile at different altitudes above the ground and the unsteady characteristics of the atmosphere (gusts and turbulence). As described in Sec. II, the whole system (balloon and mooring cable) is assumed to be subjected to a stationary mean wind profile at different altitudes above the ground. This produces a steady-state configuration in equilibrium conditions, on which the effect of the atmospheric turbulence acting on the balloon is superimposed. The unsteady characteristics of the atmosphere are considered separately as single gust and atmospheric turbulence in order to evaluate the dynamic response of the aerostat.

A. Mean Windspeed Profile

The windspeed data used in the model calculations were provided by the Natural Environment Research Council, from the Mesosphere-Stratosphere-Troposphere Radar Station located at Capel Dewi (52.42°N, 4.01°W), near Aberystwyth in west Wales, U.K. This station acquires the vertical and horizontal speeds of the wind every day, continuously, at intervals of about 3 min in time, covering the approximate altitude range of 2–20 km with a resolution of 300 m. The resulting database is an array of data that describes the windspeed variation in the time period and in the altitude range considered. For each altitude in this range, the horizontal windspeed measurements relative to the period of January–December 2007 are elaborated to obtain the mean windspeed that can be expected.

The statistical distribution used to model the data set is the Weibull probability density function $\text{Pdf}(V_{\text{Wind}})$, which is widely employed in the wind energy industry to assess the potential location of the generators [16]:

$$\text{Pdf}\,(V_{\text{Wind}}) = \frac{k}{c}\left(\frac{V_{\text{Wind}}}{c}\right)^{k-1} \exp\left[-\left(\frac{V_{\text{Wind}}}{c}\right)^k\right] \tag{8}$$

where c is the Weibull scale parameter and k is the Weibull shape parameter. To preliminarily check whether the wind data can be modeled with this kind of distribution, a graphical method based on the cumulative distribution function $\text{Cdf}(V_{\text{Wind}})$ can be applied. This function can be written as

$$\text{Cdf}\,(V_{\text{Wind}}) = 1 - \exp\left[-\left(\frac{V_{\text{Wind}}}{c}\right)^k\right] \tag{9}$$

and it can be rearranged to obtain the following expression:

$$\ell_n\{-\ell_n[1 - \text{Cdf}(V_{\text{Wind}})]\} = k\,\ell_n\,V_{\text{Wind}} - k\,\ell_n\,c \tag{10}$$

which represents a line of slope k and intercept $-k\,\ell_n\,c$.

By plotting the values of $\ell_n\{-\ell_n[1 - \text{Cdf}(V_{\text{Wind}})]\}$, obtained for the windspeed data set (Weibull probability plot), it is possible to assess if the results can be effectively approximated with a straight line and, as a consequence, if they could come from a Weibull distribution. As an example, the results obtained for the horizontal speed at an altitude of 6 km is presented in Fig. 3. The plot confirms the hypothesis that the windspeed experimental data can be modeled with the Weibull distribution. Moreover, the interpolating line can be used to determine the values of c and k.

Having determined these values, the mean and variance for each altitude can be calculated as

$$\bar{V}_{\text{Wind}} = c \cdot \Gamma\left(1 + \tfrac{1}{k}\right) \tag{11}$$

$$\sigma^2_{\text{Wind}} = c^2[\Gamma(1 + \tfrac{2}{k}) - \Gamma^2(1 + \tfrac{1}{k})] \tag{12}$$

where Γ is the gamma function [17], which allows us to determine the mean and maximum (three sigma value) windspeed for a particular height. The results obtained for each altitude up to 15 km are

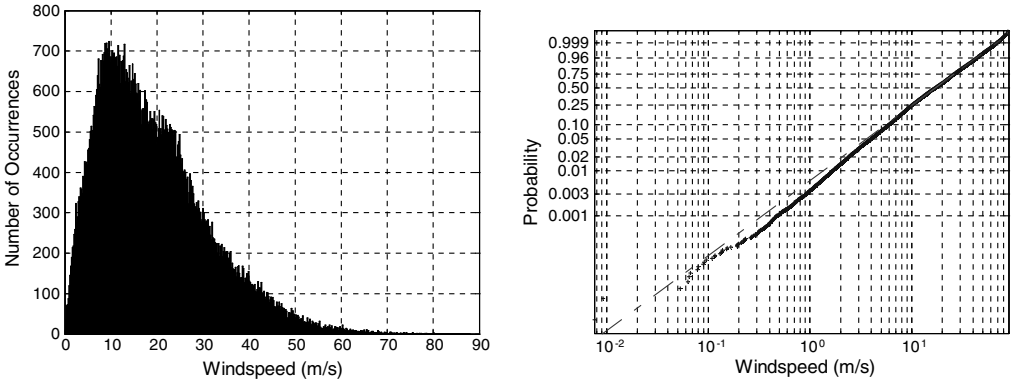

Fig. 3 Horizontal windspeed Weibull distribution (6 km altitude).

combined (fitting the data to cover the 0–2 km range) in order to obtain the mean and maximum wind profile, shown in Fig. 4.

B. Discrete Gust

A gust is defined in the *Glossary of Meteorology* [18] as "a sudden brief increase in the speed of the wind. It is more of a transient character than a squall and is followed by a lull of slackening in the windspeed." The most widely used profile to represent a single discrete gust is the (1 − cos) shape [19], defined as

$$V_{\text{Gust}} = \frac{V_{\text{Max}}}{2}\left(1 - \cos\frac{\pi \cdot x}{H}\right) \tag{13}$$

in which V_{Max} is the peak gust velocity (in meters per second), x is the penetration distance (in meters) ($0 \le x \le 2H$), and H is the discrete gust gradient length (in meters).

According to the Federal Aviation Administration Airship Design Criteria [19], the maximum gust gradient length that has to be explored is about 250 m. Moreover, for what concerns the maximum gust velocity V_{Max}, the criteria suggest a value comprised between 7.5 and 10.5 m/s, depending on the flying speed of the vehicle. In the particular case of the tethered aerostat, the flying speed cannot be univocally defined (even though it can be assumed to be equal to the relative windspeed). As a conservative assumption, the maximum gust velocity is set to 10.5 m/s for present calculations.

C. Atmospheric Turbulence

The continuous atmospheric turbulence is assumed to be a stochastic process, which can be represented in terms of statistical properties like turbulence intensity, scale length, and spectra. The method used for the simulations is based on the von Kármán model, which provides the following power spectral density representations as a function of the wave number Ω (in radians per meter), for the gust velocity in the three directions [20]:

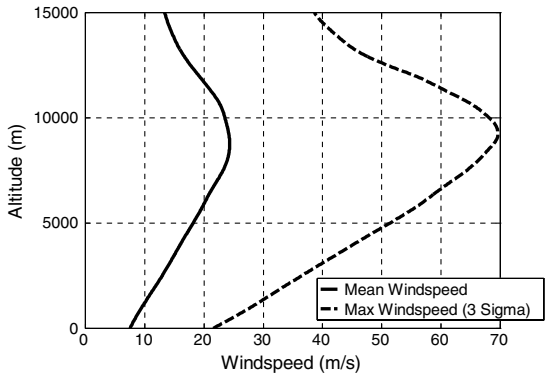

Fig. 4 Mean windspeed profile.

$$\Phi_u(\Omega) = \left(\frac{\sigma_u}{\overline{V_{\text{wind}}}}\right)^2 \overline{V_{\text{wind}}}^2 \frac{L_u}{\pi} \cdot \frac{1}{[1 + (1.339 L_u \Omega)^2]^{5/6}} \tag{14}$$

for the longitudinal direction,

$$\Phi_v(\Omega) = \left(\frac{\sigma_v}{\overline{V_{\text{Wind}}}}\right)^2 \overline{V_{\text{Wind}}}^2 \frac{L_v}{2\pi} \cdot \frac{1 + \frac{8}{3}(1.339 L_v \Omega)^2}{[1 + (1.339 L_v \Omega)^2]^{11/16}} \tag{15}$$

for the lateral direction, and

$$\Phi_w(\Omega) = \left(\frac{\sigma_w}{\overline{V_{\text{Wind}}}}\right)^2 \overline{V_{\text{Wind}}}^2 \frac{L_w}{2\pi} \cdot \frac{1 + (8/3)(1.339 L_w \Omega)^2}{[1 + (1.339 L_w \Omega)^2]^{11/16}} \tag{16}$$

for the vertical direction.

The variables L_u, L_v, and L_w represent the continuous turbulence scale length that, for altitudes above 2000 ft (≅ 600 m), can be set to 2500 ft (≅ 760 m), while the terms σ_u, σ_v, and σ_w represent the turbulence intensities in the three directions. The term $\overline{V_{\text{Wind}}}$ represents the mean windspeed at a specific altitude, as determined in Sec. III.A.

Considering a frozen field approximation for the temporal and spatial gust correlations, the three components can be generated as described in [21–23]. The method considers the following relations for the turbulence intensities in the three directions:

$$\frac{\sigma_u}{\overline{V_{\text{Wind}}}} = 0.1, \qquad \frac{\sigma_v}{\sigma_u} = 1, \qquad \frac{\sigma_w}{\sigma_u} = 1 \tag{17}$$

Moreover the method divides the wave number range of the spectrum Φ into a defined number of intervals (depending on the maximum frequency that needs to be represented) and randomly chooses a wave number for each interval to compute the value of the power spectral density. The contributions for different wave numbers are then combined to obtain the time representation of the atmospheric turbulence.

IV. Example Application

Although the method proposed is general and can be applied to any spherical tethered aerostat when subjected to operational conditions, the following sections focus on the example application of the FEM model to a specific lighter-than-air platform designed to harvest the solar power at high altitude. The aerostat is briefly described, introducing the particular configuration considered. The different atmospheric conditions are then considered, and the analysis of the system response is presented. The project also involves several nontechnical issues that have been preliminarily addressed in previous publications [11].

A. Aerostat for Electrical Power Generation

The AEPG consists of a lighter-than-air platform partially covered by PV cells that are able to collect the solar radiation at high altitude and convert it into electrical power that will be transmitted to the ground via the mooring line. Previous studies [24] have

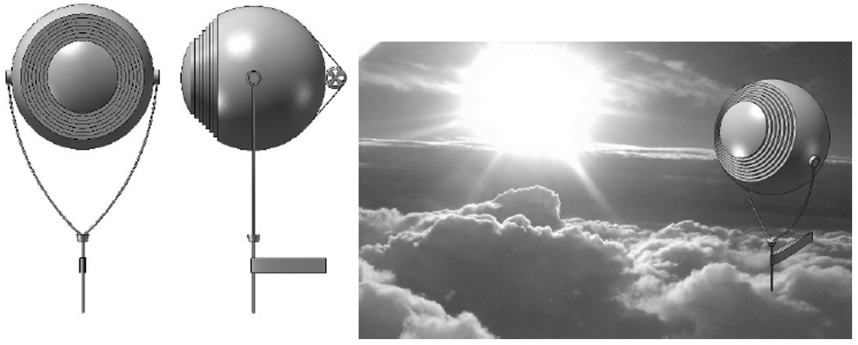

Fig. 5 AEPG concept.

demonstrated that, for a typical location in the north of Europe, a PV generator flying between 6 and 12 km could collect between 3.3 and 4.9 times the amount of energy that would be collected by the same generator on the ground. This advantage is mainly due to the combined effect of the reduced atmospheric thickness above the PV cells and the absence of cloud layers, as higher altitudes above the ground are considered. The effect of the frequent cloud coverage has always hindered the diffusion of PV systems in northern European countries (like the United Kingdom), and the AEPG proposes an innovative system to overcome this issue and increment the exploitation of the solar resource. Figure 5 shows a representation of the AEPG concept.

The present paper considers a 65-m-diam helium-filled spherical balloon, moored to the ground via a 6000-m-long tether. The choice of a spherical shape for the aerostat is due to the fact that the external surface is only partially covered by the PV cells, and the solar array needs to be pointed toward the direction of the sun in order to minimize the incidence angle of the solar beam. The pointing is performed by a gimbaled mechanism, which can provide elevation and azimuth rotations. Therefore, a spherical balloon reduces the weather-vane effect that an aerodynamically shaped aerostat would have and, as a consequence, the power requirements of the pointing mechanism. On the other hand, this shape implies a significant increase in aerodynamic drag, which needs to be taken into account when designing the mooring tether.

The definition of the drag coefficient for the aerostat, which depends on the Reynolds number value, is particularly important for the evaluation of the aerodynamic loads. For the specific application presented, the Reynolds number values are in the supercritical regime (greater than 3.5e5). In these conditions, previous studies concerning a smooth fixed sphere have demonstrated that the drag coefficient can be set to about 0.15 [25–27], while Hoerner [12] suggests a drag coefficient between 0.12 and 0.2 for a spherical balloon in supercritical flow. However, several studies [9,14,28] suggest that this value can be increased significantly due to the presence of vortex-induced vibrations in the dynamical behavior of the tethered balloon. Since the actual phase of the research is very preliminary, C_D^B is set to 0.2 for the calculations concerning the discrete gusts. Moreover, when the continuous turbulence is applied, the results obtained with drag coefficients of 0.2 and 0.8 are compared in order to estimate the influence of this parameter on the dynamic behavior of the system. Further investigations of a more accurate value for this parameter are needed in the next phases of the project through the development of computational fluid dynamic simulations and aerodynamic tests.

The main subsystem considered during the preliminary design is the PV generator, which consists of a series of solar cell arrays with a total area equal to about 75% of the projected surface of the balloon. The weight of this subsystem is determined by the value of the peak power installed and the type of solar cells employed. For the particular configuration presented in this study, the power peak is set to 0.5 MWp,and the solar cells type chosen is crystalline silicon with an efficiency of 20% and a specific power of 100 W/kg [29]. In addition to the solar cell weight, the contribution of the various collector grid components (cables, etc.) must be evaluated. This contribution is estimated as 30% of the total mass of the solar cells [30], and it is included in the evaluation of the PV system weight. The PV array is assumed to be mounted on a lightweight frame attached to the external envelope. The envelope material density usually depends on the size of the airship, since the stress in the membrane increases with the sphere diameter. As a preliminary figure, this parameter can be set to 0.5 $\mathrm{kg/m^2}$, which is the value relative to the commonly used 402 fabric provided by Lindstrand Technologies.¶

The power produced is transmitted to the ground via the mooring line, which also has the function of withstanding the forces due to the aerodynamic loads. Since the weight of the tether is crucial for the feasibility of an aerostat, this parameter has to be significantly reduced through the choice of suitable materials. Therefore, the material chosen for the part of the cable that has to withstand the loads applied is Kevlar, which provides high strength characteristics ($E = 83,000$ MPa and $\sigma_U = 3620$ MPa) as well as low density (1450 $\mathrm{kg/m^3}$). On the other hand, the material chosen for the electrical part of the cable is aluminum, which provides a resistivity of 1.82e–8 Ωm and a density of 2700 $\mathrm{kg/m^3}$. Moreover, the weight of the conductor part of the tether can also be reduced by setting the transmission voltage to high values. However, an important issue that needs to be considered when dealing with high voltages is the possible electrical breakdown of the circuit. This is particularly true when lower atmospheric densities (i.e., higher altitudes above the ground) are taken into account. For the present purposes, the transmission voltage is set to 10 kV, which keeps the weight of the conductor part of the cable and the electrical losses (5% of the power generated) to a minimum. This value for the transmission voltage can be achieved through the introduction of additional components (and additional weight), such as an inverter and a transformer. The inverter is used to convert the direct current coming from the PV panels to alternating current and then feed it into the transformer, which steps up the voltage to the value defined for transmission. The increased weight due to the presence of these components is small if compared with the reduction in tether weight.

For what concerns the remaining subsystems, they include the pointing mechanism and the buoyancy regulator, as well as lightning protection and emergency systems. In particular, the pointing mechanism consists of two electrical motors located on two opposite points along the equatorial line, which allows the elevation angle rotation. The azimuth is controlled by the rotation of a symmetric aerodynamic profile that will align itself with the wind direction. Alternatively, in the case of low windspeed, the control must be performed through the actuation of a fan located behind the balloon. On the other hand, the buoyancy regulator consists of a ballonet located inside the helium bag, which can be inflated and deflated through the actuation of a pumping system in order to adapt the gas pressure to the atmospheric one. Therefore, the remaining subsystems can constitute a significant part in the weight budget. For the moment, a reasonable figure is set between 25 and 30% of the buoyancy value. Finally, a certain amount of free lift, defined as the buoyancy value minus all the weight contributions (including the

¶Data available at http://www.lindstrandtech.com/ [retrieved 2009].

Table 1 AEPG baseline configuration parameters

Parameter	Value
Balloon diameter	65 m
System power peak	0.5 MWp
Solar cells	Crystalline silicon
Tether length	6000 m (500 segments)
Transmission voltage	10 kV
Inverter mass	3000 kg
Transformer mass	2000 kg
Transmission losses	5%
Tether safety factor	3

tether), is necessary to allow the balloon to overcome the loads induced by the environmental conditions during ascent and normal operations. A minimum value for this parameter, suggested in [5], is about 30% of the buoyancy.

A particular set of parameters describing the AEPG are assumed to perform the analysis. This configuration is considered as a baseline for the preliminary design of the system. Further evaluation of the performance of the generator will be needed in order to converge to an optimized set of design parameters.

The input parameters considered are summarized in Table 1.

B. Equilibrium Configuration

The first result to be considered is the position of the aerostat (horizontal and vertical displacements) and the equilibrium shape of the tether when the mean windspeed profile, introduced in Sec. III.A, is applied as input. These two results are presented in Fig. 6, together with the values of the inclination angles between the tether and the horizontal. The position of the balloon is 1762.3 m in the horizontal direction and 5821.5 m along the vertical, while the minimum inclination angle obtained for the node located on the ground is 71.5°.

Another important result concerns the value of the force along the tether, which is used to size the composite section (Fig. 7). The maximum force is evaluated for the node attached to the balloon.

Having calculated the values of the disposable lift at the final operational altitude, and considering the total weight of the tether (conductor and composite), the breakdown of the system weight into the various components can be defined as presented in Table 2. For the present calculations, the weight contribution of the secondary subsystems (pointing mechanism, buoyancy regulator, lightning protection, etc.), described in Sec. IV.A, is set to a fixed value of 294 kN (30 tons).

The results have been obtained for the simplified two-dimensional (2-D) case of a tethered spherical balloon subjected to a constant wind profile. Starting from the obtained equilibrium configuration, the FEM simulation will perform a full 3-D dynamic analysis of the system when the balloon is subjected to atmospheric turbulence superimposed to the constant windspeed.

It must be pointed out that the tether length is divided into 500 segments, and this value is kept constant for all the calculations presented. The choice of this figure is due to considerations about the convergence of the result, which has been assessed for different numbers of segments, showing negligible variations when more than 500 segments are considered.

C. Discrete Gust Response

As a first step in the study of the dynamic behavior of the system under analysis, the discrete gust described in Sec. III.B is applied along the three different directions (longitudinal, lateral, and vertical) with respect to the mean windspeed. After the application of the gust, the system is subjected to only the mean wind profile until the new equilibrium condition is reached, in order to analyze the complete response to the load applied. First of all, the gust is applied in the same direction as the mean windspeed, which is defined as longitudinal. The simulation is, therefore, still 2-D, since the response of the balloon will still be on the longitudinal–vertical plane. Figure 8 shows the longitudinal and vertical displacements of the balloon, relative to the steady-state position determined in Sec. IV.B. It can be noticed how the response in the longitudinal direction is overdamped, and it does not experience any evident oscillations. The same overdamped behavior can be seen in the vertical response, although a higher frequency oscillation is superimposed. From the plot, the period of oscillation can be determined, with results equal to 34.5 s.

Another important result to be considered is the maximum value of the force along the tether, obtained for the node attached to the balloon. Figure 9 shows an increment of about 9% compared with the force in equilibrium conditions. The observed period of oscillation is 34.5 s.

The results obtained when a vertical gust is applied to the balloon are shown in Figs. 10 and 11. Again, the response is on the longitudinal–vertical plane, and the absolute values of the displacements are lower than in the case of a gust in the longitudinal direction. Moreover, the period of the oscillations observed in the displacement plots are 34.5 s, as the one determined in the case of the longitudinal gust. For what concerns the value of the force, the

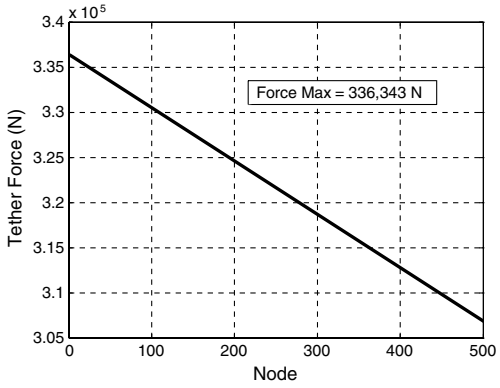

Fig. 7 Tether force (steady state).

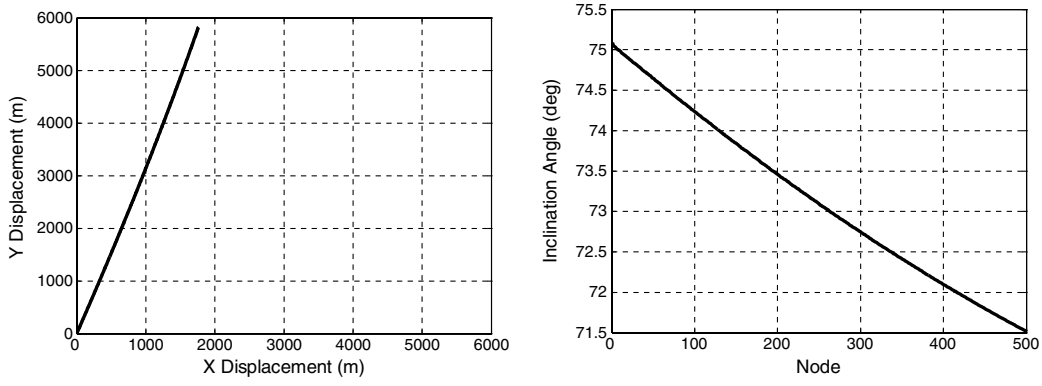

Fig. 6 Steady-state tether shape (left) and tether inclination angle (right).

Table 2 Weight breakdown for baseline configuration

	N	% of buoyancy
Buoyancy	949,311	——
Gas weight	131,137	13.8
Envelope weight	86,502	9.1
PV array weight	63,700	6.7
Tether conductor weight	10,745	1.1
Tether composite weight	23,786	2.5
Inverter weight	29,400	3.1
Transformer weight	19,600	2.1
Secondary subsystems weight	294,000	31.0
Free lift	290,442	30.6

maximum increment is about 8% compared with the steady-state case.

The application of the lateral gust results in a response of the system in the vertical–lateral plane (Fig. 12), as the oscillations in the longitudinal direction are negligible. In this case, the results include a first oscillation visible in the vertical response plot and a second one at lower frequency in the lateral direction. The higher frequency oscillation shows the same period as the previous simulations (34.5 s). The lower frequency oscillations that can be determined by the lateral displacement plot are 289.5 s. The increase of the maximum value of the force (Fig. 13) is less significant in this case (0.03%).

The periods of the oscillations determined in the three cases can be compared with the analytical solutions obtained for different

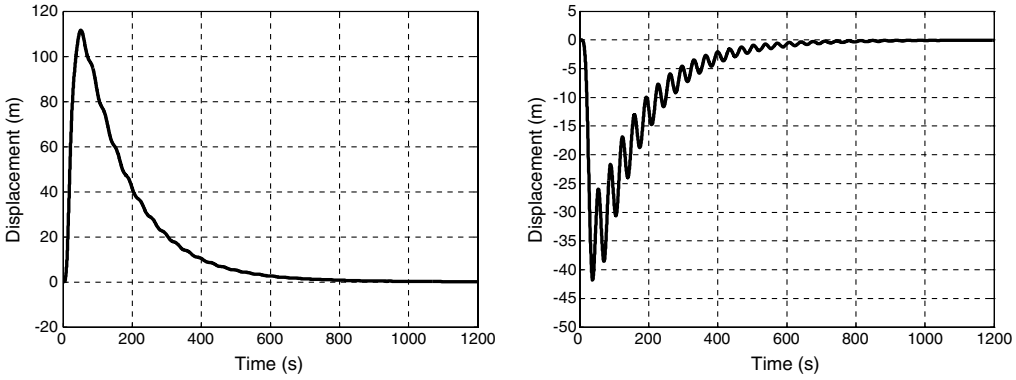

Fig. 8 Longitudinal (left) and vertical (right) system response to a longitudinal gust.

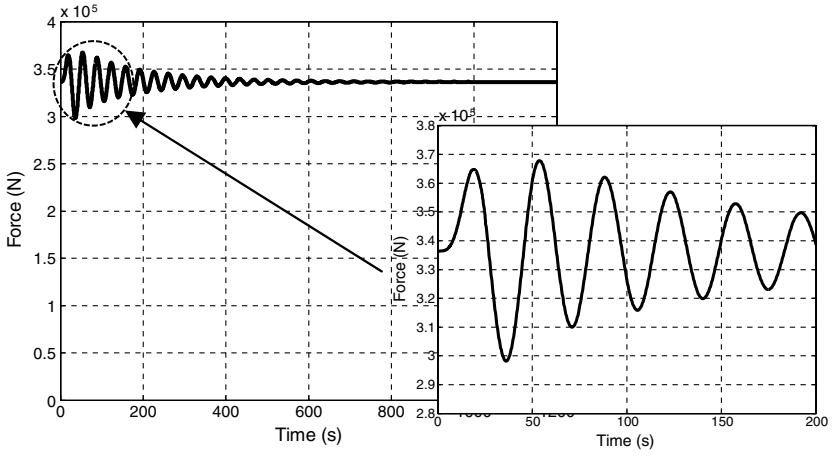

Fig. 9 Tether maximum force due to a longitudinal gust.

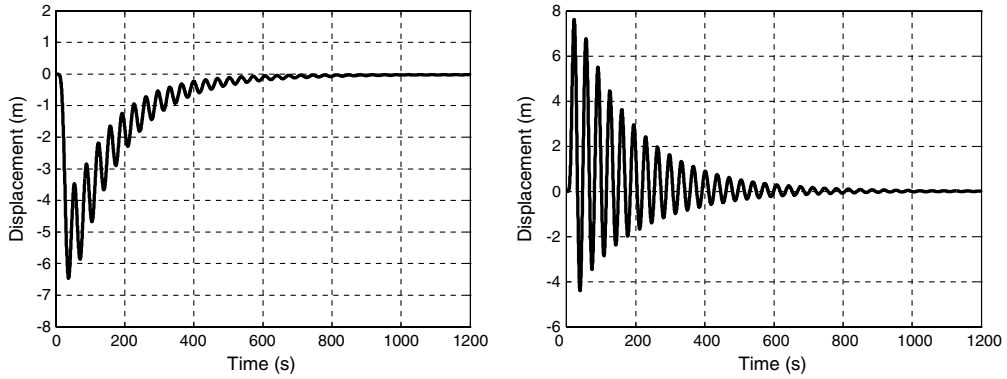

Fig. 10 Longitudinal (left) and vertical (right) system response to a vertical gust.

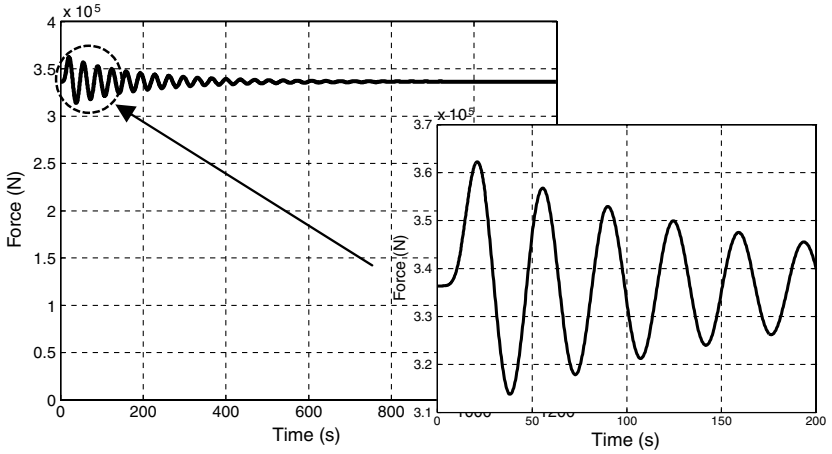

Fig. 11 Tether maximum force due to a vertical gust.

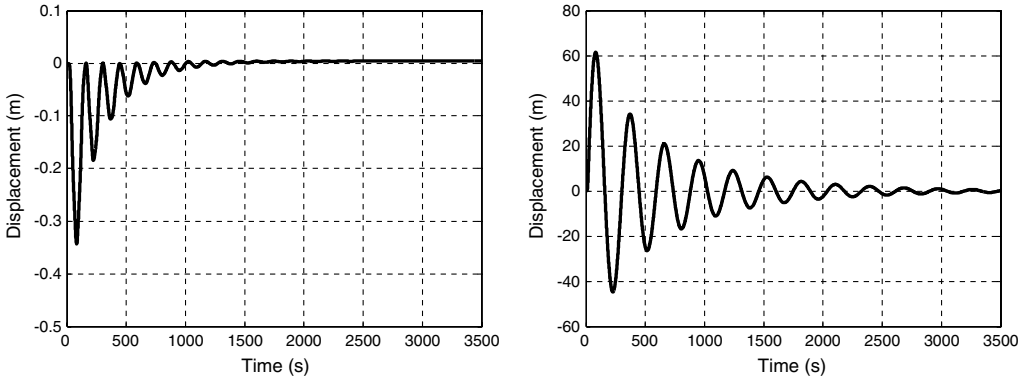

Fig. 12 Vertical (left) and lateral (right) system response to a lateral gust.

idealized cases. The frequencies for the pendulum and the axial spring modes are determined in [7] as

$$\omega_n = \sqrt{\frac{B - mg}{m_e \cdot \text{len}^{\text{tether}}}} \tag{18}$$

for the pendulum mode and

$$\omega_n = \sqrt{\frac{E_{\text{Comp}} \cdot A_{\text{Comp}}}{m_e \cdot \text{len}^{\text{tether}}}} \tag{19}$$

for the axial spring mode, where m_e is the total mass of the aerostat, which includes the value of the added mass (assumed as one half of the mass of the displaced fluid). The tether length considered is the initial value (nonstretched). The period of oscillation is determined as

$$T = \frac{2\pi}{\omega_n} \tag{20}$$

Table 3 provides the comparison between the values of the oscillation periods obtained from the simulation and the theoretical results calculated.

The comparison shows a good accordance, since the discrepancy is of 1.15% in the case of the pendulum and 1.77% in the case of the axial spring.

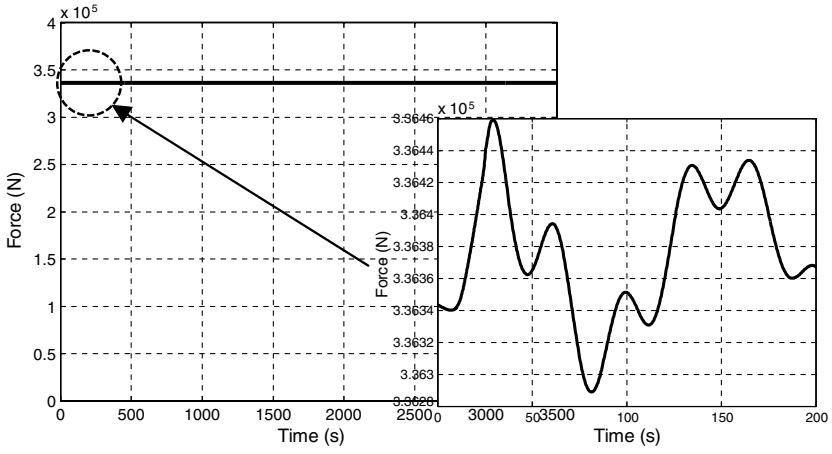

Fig. 13 Tether maximum force due to a lateral gust.

Table 3 Comparison between theory and simulation oscillation periods

	Simulation, s	Theory, s
Pendulum	289.5	286.2
Axial spring	34.5	33.9

D. Vortex-Induced Vibrations Response

Previous publications [14,28,31] have demonstrated that a tethered sphere subjected to a constant windspeed will tend to oscillate both inline and transversely to the flow direction. The amplitude of the transverse oscillation can reach a saturation value of close to one spherical diameter, while the inline oscillations are less important, leading to eight- or crescent-shaped trajectories.

In particular, the study presented in [31] identifies four different vibration modes, which are related to the formation of vortices in the wake behind the sphere. These modes are found to be functions of the reduced flow velocity defined as

$$V_{Red} = \frac{V_{\text{Wind}}}{f_N \phi_B} \tag{21}$$

where f_N is the pendulum natural oscillation frequency (in hertz). The first two modes (modes I and II) occur for reduced velocities between 5 and 10. In this range, the natural frequency of the pendulum is close to the vortex formation frequency in the wake behind the sphere. The two modes are therefore associated with a lock-in of the principal vortex shedding frequency with the body oscillation frequency. On the other hand, the third mode (mode III), described in [31], occurs at higher reduced velocities (between 20 and 40), where the vortex formation frequency is much higher than the vibration frequency. This mode is the result of a movement-induced vibration (as explained in [32]), which is responsible for an energy transfer between the fluid and the sphere for each cycle. For reduced velocities between 40 and 100, the sphere amplitude response is negligible until the fourth mode (mode IV) occurs, which is not periodic but characterized by intermittent bursts of large-amplitude vibrations. The value of reduced velocity calculated for the configuration considered in this study is 87.9, which is outside the ranges of reduced velocities of the four modes presented in [31]. However, another important result obtained in the extensive study performed by Williamson and Govardhan [14] concerns the effect of the mass ratio on the synchronization regime: i.e., the range of velocities in which the vortex-induced vibrations can occur. The mass ratio is defined as

$$m^* = \frac{m}{m_{\text{Fluid}}} \tag{22}$$

where m_{Fluid} is the mass of the displaced fluid [in kilograms]. Lower values for the mass ratio have the effect of extending the synchronization regime. Moreover, a critical value for this parameter, below which large amplitude vibrations persist to infinite reduced velocities, is determined in [14] as

$$m^*_{\text{Crit}} = 0.6 \pm 0.05 \tag{23}$$

The mass ratio value estimated for the particular configuration considered in this study is 0.6. It is therefore important to consider the possible presence of these oscillations and their effect on the system. In particular, in order to assess the technical feasibility of the generator, it is necessary to estimate the increased value of the maximum force along the tether. Considering the reduced velocity value obtained, it can be noticed that the system operates far from the flow conditions in which the lock-in occurs. As a consequence, the oscillations are assumed to belong to the movement-induced vibrations category described in [32].

The method used to model the forces responsible for the transverse vibrations is derived from [8], approximating the forces with sine functions. The magnitude of the lateral force F_0 is determined, starting from the amplitude of the lateral displacement Y_{Amp} and the value of total aerostat mass (including added mass), the system damping ratio ς, and the oscillation frequency:

$$F_0 = 2Y_{\text{Amp}} m_e \omega_n^2 \varsigma \tag{24}$$

A first estimate of the damping ratio can be derived from the results obtained in Sec. IV.C, when a lateral gust is applied to the system (Fig. 12b). The value obtained for this parameter is 0.09. The resulting sinusoidal force, determined as

$$F(t) = F_0 \sin(\omega_n t) \tag{25}$$

is applied to the system, considering an oscillation amplitude equal to the diameter of the balloon.

As the force is applied, starting from the equilibrium conditions, the first phase of the response is a transition in which the lateral oscillation amplitude increases until it reaches the value set for Y_{Amp}. The peak forces obtained in this phase are not representative of the load condition, as in the case of the single gust, and the analysis is focused on the assessment of the response in stationary conditions. The lateral displacements obtained are presented in Fig. 14. For what concerns the longitudinal displacements, the values observed are negligible compared with the lateral oscillation, and the trajectory obtained is not the typical eight shape. Moreover the increase in the maximum tether force is extremely small, as shown in Fig. 15, and it constitutes the 0.05% of the value obtained in steady-state conditions.

As a caveat, it must be pointed out that the characteristics of the system under analysis are quite different from the one considered for the study presented in [14]. In particular, the tether weight is significant and affects the value of the sag, which is negligible in the experiments described in [14]. The reduced force increase and the fact that the tethered balloon does not experience the typical eight- or crescent-shaped trajectory can be explained by the differences between the two systems.

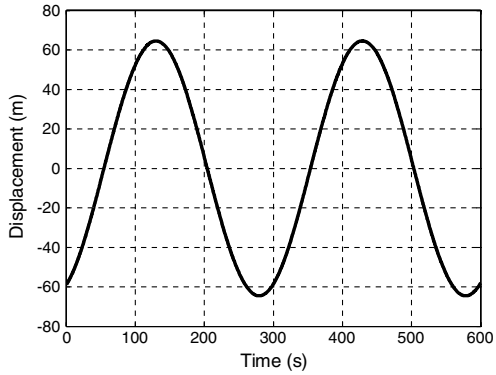

Fig. 14 Lateral displacements due to vortex-induced vibrations.

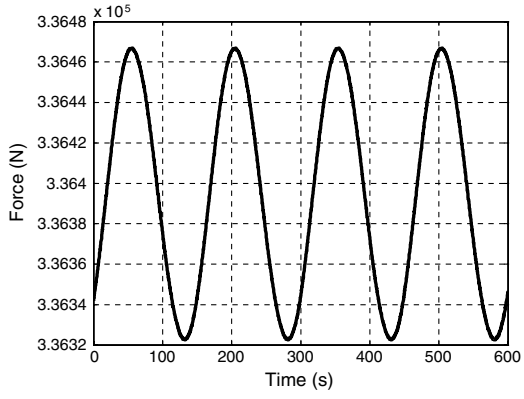

Fig. 15 Tether maximum force due to vortex-induced vibrations.

Table 4 Turbulence parameters for frequency comparison[a]

	Turbulence 1			Turbulence 2			Turbulence 3		
	Lon	Lat	Ver	Lon	Lat	Ver	Lon	Lat	Ver
N intervals	50	50	50	40	40	40	30	30	30
Max frequency, Hz	13.65	12.83	14.42	2.27	2.21	2.14	0.33	0.34	0.36
Solution ΔT, s	0.025	0.025	0.025	0.1	0.1	0.1	0.25	0.25	0.25

[a]Lon, Lat, and Ver denote longitudinal, lateral, and vertical directions, respectively.

E. Atmospheric Turbulence Response

As described in Sec. III.C, atmospheric turbulence is simulated by considering the power spectral density provided by von Kármán as a function of the wave number Ω and the mean wind velocity $\overline{V_{\text{Wind}}}$. As a first approximation, the mean wind velocity is set to 20 m/s in the following calculations, which is the value relative to an altitude of 6000 m. The wave number range of interest is divided into N intervals with an increasing width of $\Delta\Omega_i = 1.2\Delta\Omega_{i-1}$, having set the initial values to $\Omega_0 = 0.0001$ and $\Delta\Omega_0 = 0.0001$. The turbulence is generated, selecting a random wave number for each of the intervals determined. Since the wave number can be related to the turbulence frequency as $f = (\overline{V_{\text{Wind}}} \cdot \Omega)/2\pi$, the choice of a defined N number of intervals determines the maximum frequency content of the simulated turbulence.

1. *Frequency Content Evaluation*

To obtain representative results of the dynamic behavior of the system, it is important to include all the frequencies that can influence the response of the system in the range considered for the simulation. The maximum frequency selected also determines the time-step value, which needs to be small enough to avoid problems related to the aliasing of the signal. From a computational point of view, the possibility of increasing the size of time steps allows the simulation to be less time consuming, even though it might be detrimental for the accuracy of the final result. It is therefore necessary to include some preliminary exploratory calculations aimed at the identification of suitable values for the parameter N and for the simulation time step. Three different turbulence profiles are considered, setting the parameters to the values presented in Table 4. Slightly different values of the maximum frequency for the longitudinal, lateral, and vertical turbulence are due to the fact that the values are randomly selected in each interval.

It can be noticed that the lowest of the three maximum frequencies chosen (turbulence 3) is about 10 times the axial spring frequency determined in Sec. IV.C. The comparison between the three generated turbulences is presented in Figs. 16–18.

The displacements obtained in the three cases are shown in Fig. 19. It can be noticed that the results are comparable, with minimal differences, even in the case of the third turbulence.

For what concerns the maximum value of the force along the tether, obtained for the node attached to the balloon, the results are presented in Fig. 20.

As mentioned in the previous sections, the turbulence is applied after the system has reached an equilibrium condition due to the constant mean wind profile. The results therefore show an initial (10 s) high-frequency oscillatory transient. Again, the differences between the simulations are small, even though it can be seen how turbulence 3 introduces some other oscillation. The solution stabilizes after about 30 s and converges to the same results as the ones obtained with turbulences 1 and 2. The choice of using the parameters set for turbulence 3 to define the input of the model seems reasonable. This allows saving computational time while obtaining a result representative of the real situation, since higher frequencies in

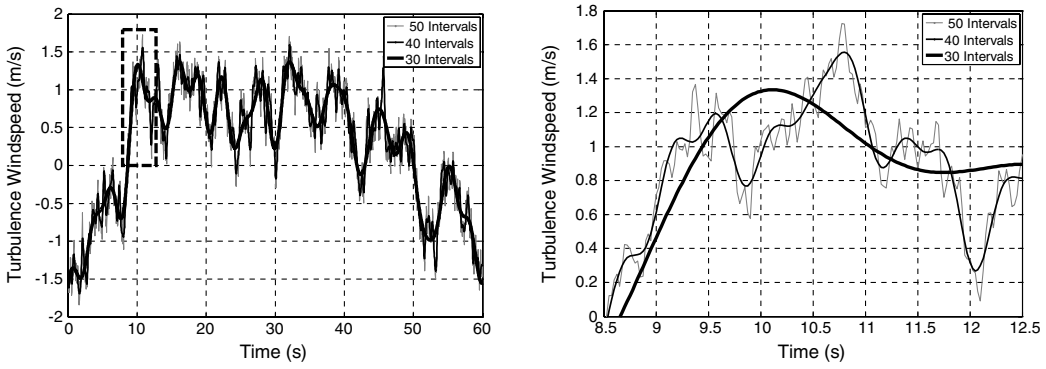

Fig. 16 Longitudinal turbulence: frequency content comparison (left: full time scale; right: detail).

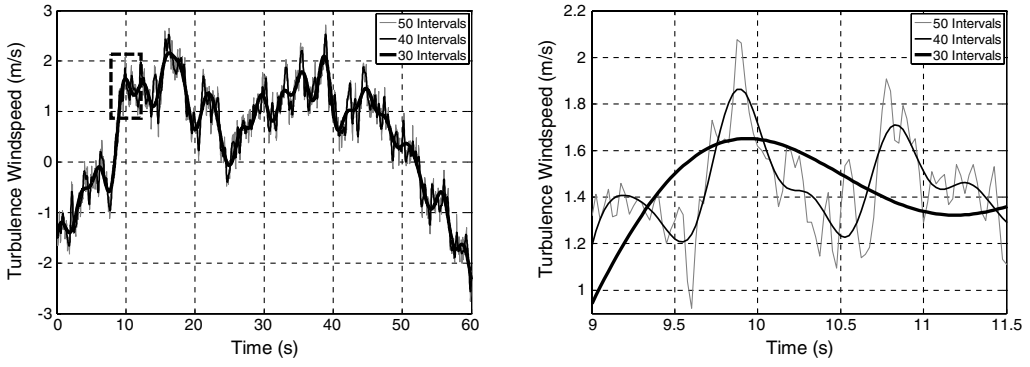

Fig. 17 Lateral turbulence: frequency content comparison (left: full time scale; right: detail).

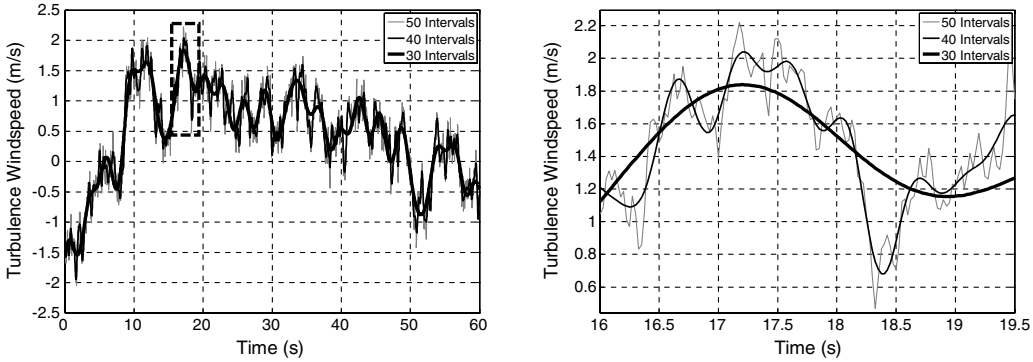

Fig. 18 Vertical turbulence: frequency content comparison (left: full time scale; right: detail).

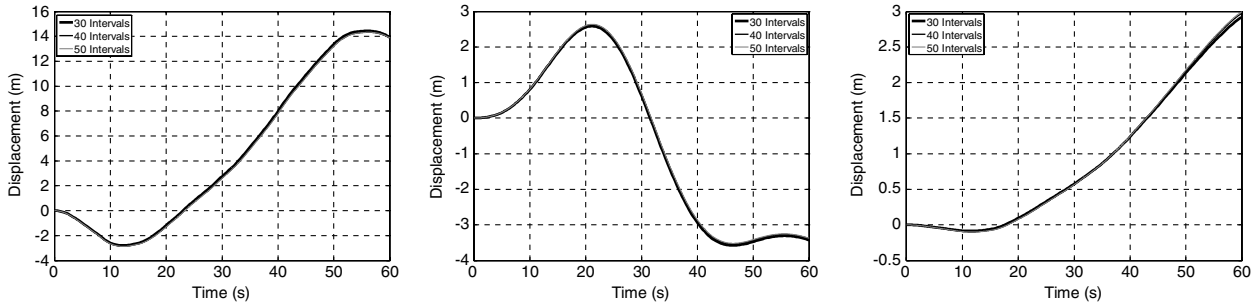

Fig. 19 Longitudinal (left), vertical (center), and lateral (right) system response to turbulence.

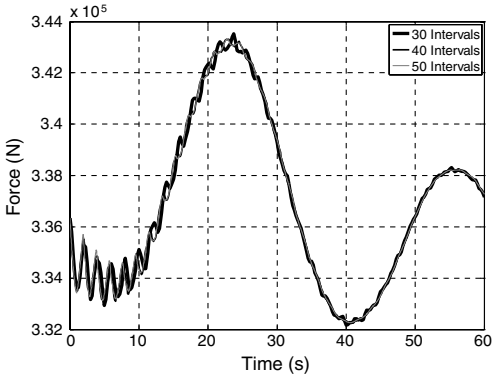

Fig. 20 Tether maximum force due to turbulence.

the input turbulence are filtered by the system. As an indication of the time necessary to perform the computations, the simulation presented in Sec. IV.E.2 required about 1 h to run on an Intel Core 2 Duo processor (3 GHz and 3.9 GB RAM).

2. *Dynamic Simulation Results*

The turbulence parameters and time step defined in the previous section are used to perform a 20 min simulation and to evaluate the response of the AEPG in realistic working conditions. As in the case of the single gust along the three directions and the vortex-induced vibrations, the results considered concern the balloon displacements and the maximum force along the mooring tether (Figs. 21–23). Moreover, the results determined considering two different values for the balloon drag coefficient (0.2 and 0.8) are compared in order to evaluate the influence of this parameter on the response of the system. It must be pointed out that the drag coefficient has a significant effect on the balloon position and final shape of the tether in steady-state conditions. The equilibrium values obtained considering $C_D^B = 0.8$ are 4800.7 and 3735.7 m for vertical and horizontal positions, respectively, while the minimum inclination angle is 50.2°. However, the present study is focused on the evaluation of the behavior of the tethered platform when subjected to realistic operating conditions, and the results are therefore focused on the dynamic response evaluated, starting from the steady-state configuration.

For what concerns the longitudinal displacements, the absolute values obtained are less than 100 m, and the effect of the increased drag coefficient is not significant. On the other hand, the effect of the increased balloon drag coefficient appears more evident when evaluating the vertical displacements, where the maximum values obtained are 30 m for $C_D^B = 0.2$ and 80 m for $C_D^B = 0.8$. A similar effect can be observed in the case of the lateral direction, where the magnitude of the displacements is comparable with the vertical (30 and 50 m). To assess the technical feasibility of the system, it is important to compare the absolute values of the displacements

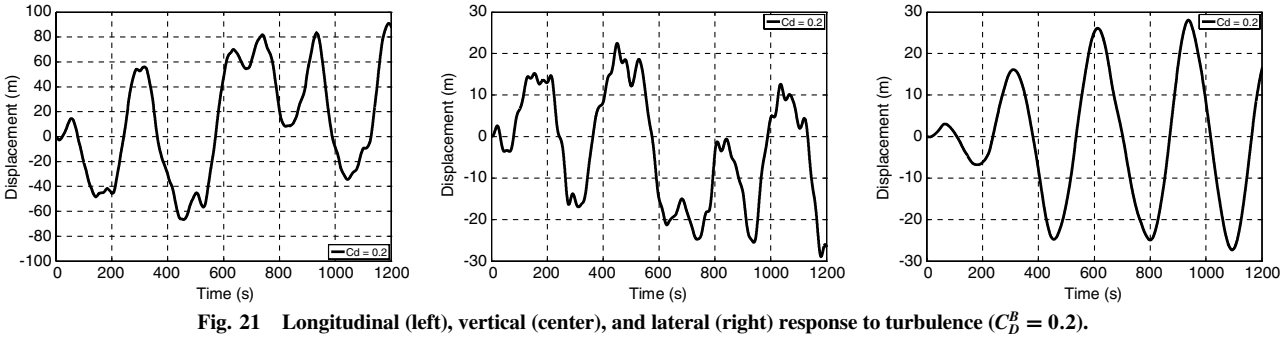

Fig. 21 Longitudinal (left), vertical (center), and lateral (right) response to turbulence ($C_D^B = 0.2$).

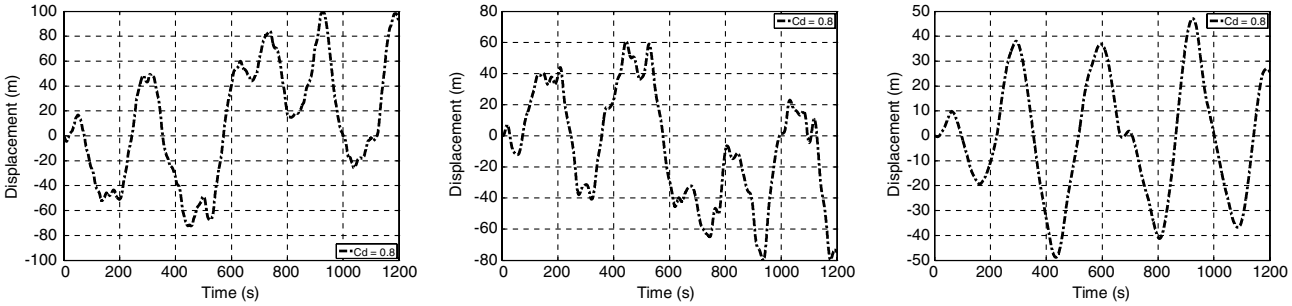

Fig. 22 Longitudinal (left), vertical (center), and lateral (right) response to turbulence ($C_D^B = 0.8$).

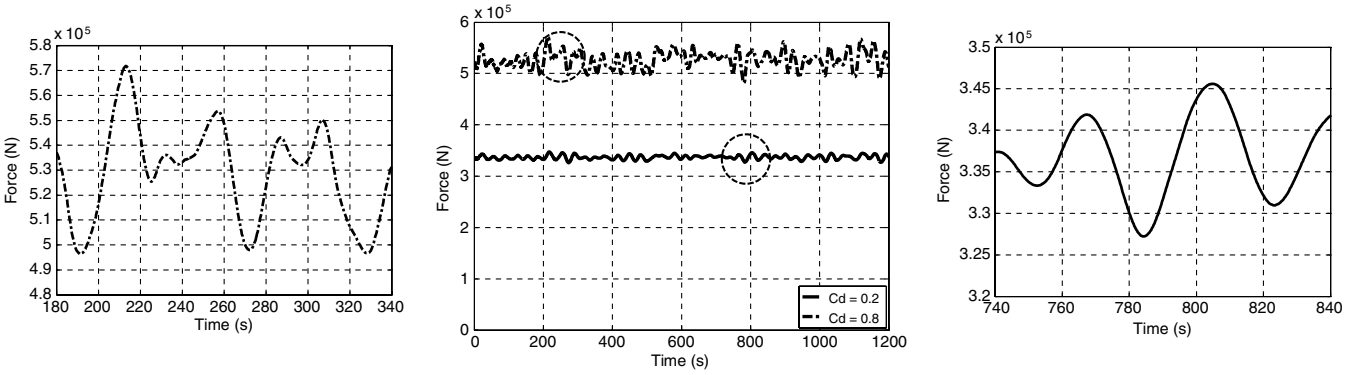

Fig. 23 Tether maximum force due to turbulence.

obtained with the application of the 3-D turbulence to the position determined in steady-state conditions. The longitudinal oscillations represent 5.7 and 2.7% of the equilibrium position for the two drag coefficients considered, while the amplitude of the vertical displacements are less than 0.5 and 1.7% of the steady-state altitude value.

Finally, the forces presented in Fig. 23 show an oscillation about the steady-state value that produces an increase in the tether tension. The maximum increase can be estimated from the peak forces as 3.3% of the equilibrium value in the case of low balloon drag and 9% in the case of high drag coefficient.

The response to a discrete gust, presented in Sec. III.B, has highlighted the presence of two oscillation modes: i.e., lateral pendulum and axial spring with two specific frequencies of 0.0035 and 0.029 Hz in the case of $C_D^B = 0.2$. Figures 21 and 23 show some characteristic oscillations for which the frequencies can be determined by the time distances between the peaks. In particular, the results obtained for the lateral displacement (0.0034 Hz) and for the tether force (0.031 Hz) demonstrate that the two oscillation modes are still represented in the continuous turbulence simulation.

The figures presented in this section quantify the dynamic response of the system in terms of displacements and tether forces contributing to the assessment of the technical feasibility of the AEPG. On the basis of the results obtained, it can be inferred that the dynamic behavior of the system does not constitute a show stopper for the development of the flying generator.

V. Conclusions

This paper introduces a FEM approach to the study and analysis of the dynamical behavior of a tethered lighter-than-air balloon subjected to atmospheric operational conditions. The method proposed is based on a relatively simple FEM of the system developed with commercial software embedded in loop that processes the atmospheric parameters (such as turbulence 3-D profile) and produces a nonlinear simulation of the dynamic response of the system. In particular, the present study presents the complete analysis of the dynamic response of a tethered lighter-than-air platform equipped with a solar array for the production of electric power from the sun. The FEM therefore constitutes a useful tool, employed to preliminarily assess the technical feasibility of this kind of system.

The input values (windspeed) are derived by experimental and simulated data, which define the mean windspeed profile and the characteristics of discrete gusts and continuous atmospheric turbulence. Moreover, the possible effect of vortex-induced vibrations is also investigated, as well as the influence of the value set for the balloon drag coefficient. The main outputs considered in the analysis are the balloon displacements and the maximum value of the force along the tether. In particular, the application of the single gust leads to the determination of the frequencies of two oscillation modes (lateral pendulum and axial spring), which are compared with theoretical results, showing good agreement. On the other hand, the application of the simulated continuous turbulence is used to assess the dynamic response of the system in realistic operational conditions. The results show the presence of the two oscillation modes, mentioned previously, and demonstrate the filtering effect of the system, which can be used to determine the time step employed in the simulation.

Finally, the model outputs are assessed in order to identify possible critical areas for the technical feasibility of the system under analysis. The figures obtained under the conditions assumed for the simulation do not constitute a show stopper for the further development of the design and the viability of the concept.

Acknowledgments

The authors would like to acknowledge the support of the Mesosphere-Stratosphere-Troposphere Radar Facility at Aberystwyth, funded by the United Kingdom Natural Environment Research Council and the British Atmospheric Data Centre, for providing the data concerning the wind statistics.

References

[1] "Tethered Aerostat Radar System," U.S. Air Force, Air Combat Command, Langley AFB, VA, Feb 2006.

[2] Bely, P., and Ashford, R. L., "High-Altitude Aerostats as Astronomical

Platforms," *Proceedings of the SPIE: The International Society for Optical Engineering*, Vol. 2478, SPIE, Bellingham, WA, 1995, pp. 101–116.
doi:10.1117/12.210916

[3] DeLaurier, J. D., "A Stability Analysis for Tethered Aerodynamically Shaped Balloons," *Journal of Aircraft*, Vol. 9, No. 9, 1972, pp. 646–651.
doi:10.2514/3.59054

[4] Jones, S. P., and Krausman, J. A., "Nonlinear Dynamic Simulation of a Tethered Aerostat," *Journal of Aircraft*, Vol. 19, No. 8, 1982, pp. 679–686.
doi:10.2514/3.57449

[5] Badesha, S. S., Euler, A. J., and Schroder, L. D., "Very High Altitude Tethered Balloon Parametric Sensitivity Study," 34th AIAA Aerospace Sciences and Exhibit, Reno, NV, AIAA Paper 1996-0579, 1996.

[6] Badesha, S. S., and Bunn, J. C., "Dynamic Simulation of High Altitude Tethered Balloon System Subject to Thunderstorm Windfield," AIAA Atmospheric Flight Mechanics Conference and Exhibit, Monterey, CA, AIAA Paper 2002-4614, 2002.

[7] Lambert, C., and Nahon, M., "Stability Analysis of a Tethered Aerostat," *Journal of Aircraft*, Vol. 40, No. 4, 2003, pp. 705–715.
doi:10.2514/2.3149

[8] Coulombe-Pontbriand, P., and Nahon, M., "Experimental Testing and Modelling of a Tethered Spherical Aerostat in an Outdoor Environment," *Journal of Wind Engineering and Industrial Aerodynamics*, Vol. 97, Nos. 5–6, 2009, pp. 208–218.
doi:10.1016/j.jweia.2009.06.005

[9] Miller, J. I., and Nahon, M., "Analysis and Design of a Robust Helium Aerostats," *Journal of Aircraft*, Vol. 44, No. 5, 2007, pp. 1447–1458.
doi:10.2514/1.25627

[10] Aglietti, G. S., "Dynamic Response of a High Altitude Tethered Balloon System," *Journal of Aircraft*, Vol. 46, No. 6, 2009, pp. 2032–2040.
doi:10.2514/1.43332

[11] Aglietti, G. S., Redi, S., Tatnall, A. R., and Markvart, T., "Harnessing High Altitude Solar Power," *IEEE Transactions on Energy Conversion*, Vol. 24, No. 2, 2009, pp. 442–451.
doi:10.1109/TEC.2009.2016026

[12] Hoerner, S. F., *Fluid Dynamic Drag*, Hoerner Fluid Dynamics, Albuquerque, NM, 1965.

[13] Dorrington, G. E., "Use of Helium-Filled Dirigibles for Scientific Exploration of Rain Forest Canopy," *7th International Airship Convention*, Friedrichshafen, German Soc. for Aeronautics and Astronautics (DGLR), Bonn, 9–11 Oct. 2008.

[14] Williamson, C. H. K., and Govardhan, R., "Vortex Induced Vibrations," *Annual Review of Fluid Mechanics*, Vol. 36, No. 1, 2004, pp. 413–455.
doi:10.1146/annurev.fluid.36.050802.122128

[15] "U.S. Standard Atmosphere," U.S. Government Printing Office, Washington, D. C., 1976.

[16] Seguro, J. V., and Lambert, T. W., "Modern Estimation of the Parameters of the Weibull Wind Speed Distribution for Wind Energy Analysis," *Journal of Wind Engineering and Industrial Aerodynamics*, Vol. 85, No. 1, 2000, pp. 75–84.
doi:10.1016/S0167-6105(99)00122-1

[17] Askey, R. A., and Roy, R., "Gamma Function," *Digital Library of Mathematical Functions* [online], 2010, National Institute of Standards and Technology, Gaithersburg, MD, http://dlmf.nist.gov/5 [retrieved 2010].

[18] Huschke, R. E., *Glossary of Meteorology*, American Meteorological Soc., Boston, 1959.

[19] "Airship Design Criteria," Federal Aviation Administration, Policy FAA-P-8110-2, 1986.

[20] "Flying Qualities of Piloted Airplanes," U.S. Department of Defense, MIL-SPEC MIL-F-8785C, 5 Nov. 1980.

[21] Nahon, M., Gilardi, G., and Lambert, C., "Dynamics/Control of a Radio Telescope Receiver Supported by a Tethered Aerostat," *Journal of Guidance, Control, and Dynamics*, Vol. 25, No. 6, 2002, pp. 1107–1115.
doi:10.2514/2.4990

[22] Etkin, B., *Dynamics of Atmospheric Flight*, Wiley, New York, 1972.

[23] Kang, W., and Lee, I., "Analysis of Tethered Aerostat Response Under Atmospheric Turbulence Considering Nonlinear Cable Dynamics," *Journal of Aircraft*, Vol. 46, No. 1, 2009, pp. 343–347.
doi:10.2514/1.38599

[24] Redi, S., Aglietti, G. S., Tatnall, A. R., and Markvart, T., "An Evaluation of a High Altitude Solar Radiation Platform," *Journal of Solar Energy Engineering*, Vol. 132, No. 1, 2010, pp. 1–8.
doi:10.1115/1.4000327

[25] Schlichting, H., *Boundary Layer Theory*, 7th ed., McGraw–Hill, New York, 1979.

[26] Achenbach, E., "Experiments on the Flow Past Spheres at Very High Reynolds Numbers," *Journal of Fluid Mechanics*, Vol. 54, No. 3, 1972, pp. 565–575.
doi:10.1017/S0022112072000874

[27] Maxworthy, T., "Experiments on the Flow Around a Sphere at High Reynolds Numbers," *Journal of Applied Mechanics*, Vol. 36, No. 3, 1969, pp. 598–607.

[28] Govardhan, R., and Williamson, C. H. K., "Vortex-Induced Motions of a Tethered Sphere," *Journal of Wind Engineering and Industrial Aerodynamics*, Vols. 69–71, July–Oct. 1997, pp. 375–385.
doi:10.1016/S0167-6105(97)00170-0

[29] Green, M. A., Emery, K., Hishikawa, Y., and Warta, W., "Solar Cell Efficiency Tables (Version 32)," *Progress in Photovoltaics: Research and Applications*, Vol. 16, No. 5, 2008, pp. 435–440.
doi:10.1002/pip.842

[30] Khoury, G. A., and Mowforth, E., A Solar Airship: More Than a Flight Of Fancy, *NewScientist*, Vol. 79, No. 1111, 1978, pp. 100–102.

[31] Jauvtis, N., Govardhan, R., and Williamson, C. H. K., "Multiple Modes of Vortex Induced Vibration of a Sphere," *Journal of Fluids and Structures*, Vol. 15, Nos. 3–4, April 2001, pp. 555–563.
doi:10.1006/jfls.2000.0348

[32] Naudascher, E., and Rockwell, D., *Flow Induced Vibrations: An Engineering Guide*, Balkema, Boca Raton, FL, 1993.